Accepted Manuscript

Title: Selective Epoxidation of Cyclohexene with Molecular Oxygen on Catalyst of Nanoporous Au Integrated with MoO$_3$ Nanoparticles

Author: Jian Dou Franklin Feng Tao

Please cite this article as: Jian Dou, Franklin Feng Tao, Selective Epoxidation of Cyclohexene with Molecular Oxygen on Catalyst of Nanoporous Au Integrated with MoO3 Nanoparticles, Applied Catalysis A, General http://dx.doi.org/10.1016/j.apcata.2016.10.010

Selective Epoxidation of Cyclohexene with Molecular Oxygen on Catalyst of Nanoporous Au Integrated with MoO₃ Nanoparticles

Jian Dou[a,b], Franklin (Feng) Tao[a,b,]*

[a] Department of Chemical and Petroleum Engineering, University of Kansas, Lawrence, KS, 66045, USA
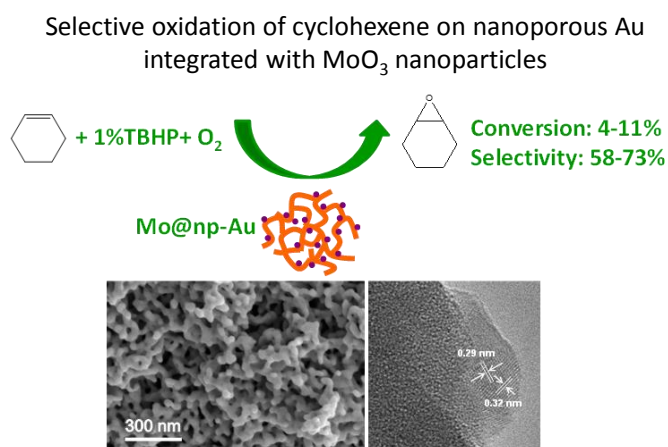
[b] Department of Chemistry, University of Kansas, Lawrence, KS 66045, USA

* To whom all correspondences should be sent to. Email: franklin.feng.tao@ku.edu.

Corresponding Author

*Email: franklin.feng.tao@ku.edu

Graphical abstract

Selective oxidation of cyclohexene on nanoporous Au
integrated with MoO_3 nanoparticles

+ 1%TBHP+ O_2 → Conversion: 4-11%
Selectivity: 58-73%

Mo@np-Au

300 nm   0.29 nm   0.32 nm

Research highlights

- MoO_3@np-Au catalyst is active for selective oxidation of cyclohexene with molecular oxygen.
- MoO_3@np-Au catalysts exhibited high selectivity of 58%-73% for cyclohexene oxide at conversion of 4%-11% of cyclohexene.
- MoO_3@np-Au catalyst behaves as a bi-functional catalyst.

2

Abstract

Selective oxidation of olefins to desired products such as epoxides is highly demanded in chemical industry. It remains challenging to achieve high selectivity for production of epoxides over heterogeneous catalysts through using molecular oxygen as the oxidant. Nanoporous reverse catalysts (MoO_3@np-Au) consisting of pure nanoporous gold (np-Au) and MoO_3 nanoparticles anchored on Au ligaments were synthesized for selective oxidation of cyclohexene with molecular oxygen. By controlling the loading of molybdenum and thermal treatment condition, MoO_3 nanoparticles with size of ~5 nm were uniformly anchored on the surface of gold ligaments (30-50 nm) of pure nanoporous gold (np-Au). These synthesized MoO_3@np-Au catalysts exhibited high selectivity of 58%-73% for production of cyclohexene oxide at conversion of 4%-11% of cyclohexene by using molecular oxygen as the oxidant. Compared to MoO_3@np-Au, the selectivity for the production of cyclohexene oxide on pure np-Au catalyst is only 6% under the same catalytic condition as that on MoO_3@np-Au. The observed high selectivity for production of cyclohexene oxide on MoO_3@np-Au can be rationalized with a bi-functional mechanism of a reverse metal/oxide catalyst. The in-situ formed surface molybdenum oxo-peroxo species are suggested to be responsible for selective oxidation of cyclohexene to cyclohexene oxide, while the MoO_3/Au interface activates molecular oxygen to regenerate the molybdenum oxo-peroxo active centers.

3

1. Introduction

Selective oxidation of olefins is an extremely important reaction in chemical industry.[1] For instance, the oxidized products such as epoxides are widely used for production of resins, paints, surfactants and intermediates for organic synthesis.[2] Epoxidation of the simplest olefins, ethylene to ethylene oxide has long been established in industry by reacting ethylene with molecular oxygen over silver catalysts. However, it remains challenging for direct oxidation of higher olefins such as propylene and cyclohexene using molecular oxygen instead of peroxide as oxidant.[3] Generally, oxidation of higher olefins can proceed with various molecular catalysts or supported metal catalysts through using peroxides such as hydrogen peroxide or tert-butyl hydroperoxide as an oxidant[4-9]. However, the high cost of peroxide oxidants and costly footprint of handling large amount of peroxides have a considerable influence on whether oxidation of higher olefins such as cyclohexene should be processed with peroxides at industrial scale or not.[10-17] Molecular oxygen, a cheap and readily available gas is definitely a green, low-cost oxidant for selective oxidation reactions. Thus, it is highly desirable to develop a catalyst active for *selective* epoxidation of cyclic olefins using molecular oxygen at a mild condition.

Gold-based catalysts have been widely used for selective oxidation of olefins.[18-30] For example, activated carbon supported gold nanoparticles with size of 5-50 nm have been successfully utilized for oxidation of cyclohexene with hydroperoxide as oxidant by using 1,2,3,4-tetramethylbenzene as solvent.[18] In addition, gold nanoparticles with a size less than 10 nm supported on modified silica supports were effective in oxidation of cyclohexene using only molecular oxygen as the oxidant [19-21]; however, the selectivity for production of cyclohexene oxide (or called epoxide) on these catalysts is only about 9-14%.[19,21]

4

Oxidation of cyclohexene has also been investigated under solvent free conditions.[31-34] For example, using silica or manganese oxide supported gold catalysts, selectivity for production of epoxide (i.e., cyclohexene oxide) is generally lower than 10% when molecular oxygen was used.[31,32] In order to improve the selectivity for production of cyclohexene oxide, gold nanoclusters (i.e., Au_9 and Au_{101}) were anchored onto WO_3 nanoparticles[35]; the selectivity for production of cyclohexene oxide on Au_{101}/WO_3 catalyst was improved largely to 35% comparing to 7% of Au_{101}/SiO_2 catalyst when molecular oxygen or peroxide is used as the oxidant.[35] This difference suggests the promotion effect of the support, WO_3 on catalytic selectivity of cyclohexene oxide. Even though these efforts have been made in using molecular oxygen as oxidant and a reasonable conversion of cyclohexene in selective oxidation has achieved, high selectivity for production of epoxides by using molecular oxygen as an oxidant in a solvent free condition has still remained challenging.

It is well known that MoO_3-based catalyst is efficient in selective oxidation of hydrocarbon while peroxide is used as the oxidant. For example, epoxidation of cyclohexene on $Mo^{VI}O_3$ supported on silica using hydrogen peroxide or tert-butyl hydroperoxide as the oxidant was investigated. Furthermore, molybdenum based oxides and heteropolyacids have been reported as excellent promoter or support for noble metals (i.e., Pt and Au) for hydrogenation, water gas shift and electrochemical reactions.[36-40] As reported in literature, np-Au is highly active in activating molecular oxygen;[41,42] this activated molecular oxygen can spillover to surface of MoO_3 where oxidization of cyclohexene to products is performed. Thus, we expect that the integration of MoO_3 nanoparticles on internal surface of ligaments of np-Au could tune catalytic performances of np-Au in selective oxidation of cyclohexene with molecular oxygen.

Here we synthesized the catalyst MoO_3@np-Au consisting of np-Au and MoO_3 nanoparticles anchored on Au ligaments in the pores of np-Au through different pre-treatments of the catalyst precursor. They exhibit selectivity up to 73% for epoxidation of cyclohexene to cyclohexene oxide which is much higher than pure np-Au.

2. Experimental

2.1 Synthesis of nanoporous gold catalysts.

Nanoporous gold sponge (np-Au) was synthesized following literature method.[43] In a typical synthesis of np-Au sponge nanocatalyst, 10 mL of 4.5 mM polyvinylpyrrolidone (PVP, $(C_6H_9NO)_n$, Sigma-Aldrich) solution (50 mg PVP in 100 mL ethanol, C_2H_5OH, Sigma-Aldrich) was mixed with 10 mL of 30 mM gold (III) chloride hydrate ($HAuCl_4 \cdot xH_2O$, Sigma-Aldrich) solution, followed by stirring at room temperature for 15 min. After that, 10 mL of freshly prepared 0.1 M sodium borohydride ($NaBH_4$, Sigma-Aldrich) was poured rapidly into the mixed solution under stirring. The mixture was further stirred for 15 min before centrifuged and then washed with deionized water. The solid product was dried at room temperature for overnight, and was denoted as np-Au. The catalyst with integrated np-Au and Mo was prepared by impregnation with ammonium heptamolybdate ($(NH_4)_6Mo_7O_{24} \cdot 4H_2O$, Alfa Aesar) solution. The impregnated samples were dried at 60°C followed by calcination in statiC-air and/or hydrogen ($5\%H_2$/Ar, Prax Air) at 300°C for 1 h. The final samples were denoted as X%Mo@np-Au-T (X = 1.0 and 2.0, which stands for the percentage of loading of Mo, T stands for the calcination temperature).

2.2 Selective oxidation of cyclohexene.

Liquid phase oxidation of cyclohexene was carried out in an autoclave with a capacity of 100 mL, on which K-type thermocouple and pressure gauge were integrated. The probe of thermocouple was submerged to the liquid for an accurate measurement of catalytic temperature. In a typical run, 15 mL of cyclohexene was mixed with 0.5 mL of undecane ($C_{11}H_{24}$, as an internal standard, Sigma-Aldrich), followed by adding 10 mg of catalyst and 0.27 mL of tert-butyl hydroperoxide solution (TBHP, $C_4H_{10}O_2$, 5.5 M in decane, Sigma-Aldrich). The mole ratio of TBHP to cyclohexene was fixed at 1/100. The reaction proceeded under vigorous stirring at 80°C for 4 h. Gas chromatography–mass spectrometry (GC-MS, Agilent, 6890N) was used for qualitatively identification of reaction products. Quantitative determination of oxidation products (i.e., cyclohexene oxide, 2-cyclohexen-1-ol, and 2-cyclohexen-1-one) was achieved with gas chromatography equipped with a flame ion detector (FID) and a Restek packed column (30 m × 0.32 mm × 0.25 μm). Commercial samples of cyclohexene oxide, 2-cyclohexen-1-ol, and 2-cyclohexen-1-one were used as external standards for calibration of GC peaks. The concentration of cyclohexenyl hydroperoxide was determined by iodometric titration method.[44] Typically, 0.5 mL of analyte was mixed with 40 mL of isopropyl alcohol and 2 mL of acetic acid, followed by heating to reflux. After that, 2.00 g of sodium iodide was dissolved in 10 mL of isopropyl alcohol, which was then added to the above solution. The resulted mixture was further refluxed for 5 min, followed by adding 5 mL of deionized water and titrated with 0.100 M sodium thiosulfate.

2.3 Materials characterization.

The crystallographic structure of the solid samples was investigated using a Bruker X8 Proteum diffraction system equipped with Helios multilayer optics, and APEX II CCD detector and a Bruker MicroStar microfocus rotation anode X-ray source (Cu K_α radiation, $\lambda = 1.54178$ Å) operating at 45 kV and 60 mA. Powders were suspended in Paratone N oil and placed into a nylon loop and mounted on a goniometer head. The sample was scanned at a rotation rate of 2º/second. The dimension, morphology, and chemical composition of the solid samples were examined using scanning electron microscopy (Versa 3D dual beam, FEI) with a silicon drift energy dispersive X-ray detector (Oxford Instruments), and high resolution transmission electron microscopy (HRTEM/EDX, FEI Tecnai F20, 200 kV; and Zeiss Libra 200-80, 200 kV). The TEM samples were prepared by dispersion of nanoporous gold catalysts in ethanol under sonication for 10 min. The suspension was dropped onto a copper mesh grid with lacey carbon film, followed by drying at room temperature in air. Surface and texture properties of the samples were studied by nitrogen adsorption-desorption isotherms (Quantachrome NOVA 2200e system) at 77 K. Prior to measurements, the samples were degassed at 120ºC for 6 h. Specific surface areas of the samples were determined using Brunauer-Emmett-Teller (BET) method. The Mo loading in Mo/np-Au catalysts were determined by optical emission spectroscopy with inductively coupled plasma as excitation source (ICP-OES, Horiba Jobin Yvon JY 2000).

3. Results and Discussion

3.1 Preparation and characterization of catalyst of np-Au with integrated MoO_3 nanoparticles (MoO_3@np-Au)

Pure nanoporous gold (np-Au) was synthesized through a wet chemistry route using PVP as surfactant and capping agent in water/ethanol mixed solvent (Figure 1). The crystallinity of as-prepared nanoporous gold was examined with XRD. As shown in Figure S1, peaks at 38.3, 44.4, 64.6, 77.8, and 82.0° were attributed to (111), (200), (220), (311), and (222) plane of metallic gold with a face centered cubic phase (JCPDS 04-0784, space group: Fm-3m, $a_0 = b_0 = c_0 = 4.0786$ Å). The morphology of as-prepared nanoporous gold material was characterized by SEM. As presented in Figure S2, the nanoporous gold consisted of interlinked gold ligaments with diameter of 30-45 nm. The void space between gold ligaments formed the porous structure with pore diameter in the range of 30-60 nm.

In order to functionalize the nanoporous gold for selective oxidation of cyclohexene reaction, molybdenum oxide was deposited into the internal surface of np-Au via impregnation. The impregnated sample was calcined at 200-300°C for 1 h to decompose molybdenum precursor to form molybdenum oxide nanoparticles on the surface of nanoporous gold. Generally, nanoporous gold materials are thermally stable up to 300°C; coarsening of gold ligaments occurs when calcination temperature is above 300°C.[45-47] On the other hand, the decomposition temperature of ammonium heptamolybdate is 190°C. Thus, the calcination temperatures of 200 and 300°C were chosen in this work; they are high enough to decompose the molybdenum precursor to form molybdenum oxide without obvious change of the nanoporous structure of np-Au.

As shown in Figure 2, the porous structure of 1.0wt%Mo@np-Au-200°C catalyst was similar to the as-synthesized pure nanoporous gold (Figure S2). The size of gold ligament of 1.0wt%Mo@np-Au-200°C was about 30-50 nm. The void space between the gold ligaments formed the porous structure. The porosity of pure and molybdenum oxide doped nanoporous gold catalysts were examined by nitrogen adsorption-desorption method. As shown in Table 1, the specific surface area and pore volume of the as-synthesized pure nanoporous gold was 2.9 m^2/g and 0.078 mL/g, respectively. After doping with 1.0 wt% and 2.0 wt% molybdenum precursor, the specific surface area decreased to 2.8 and 2.3 m^2/g, and total pore volume decreased to 0.047 and 0.023 mL/g, respectively. The decrease in surface area and total pore volume is due to deposition of molybdenum oxide nanoparticles into the nanopores of gold sample. In order to confirm that molybdenum oxide was deposited onto nanoporous gold, the prepared MoO_3@np-Au catalysts were examined by EDX mapping. As shown in Figure 2c-e, molybdenum element was uniformly dispersed on the surface of nanoporous gold. Quantitative determination of molybdenum loading was carried out by ICP analysis. Concentration of molybdenum was measured as 0.98wt% and 2.05wt% for 1.0wt%Mo@np-Au and 2.0wt%Mo@np-Au, respectively (Table 1). The morphology of deposited molybdenum oxide was characterized by HRTEM. As shown in Figures 3a and 3b, MoO_3 nanoparticles with size of ~ 5 nm were dispersed on the surface of nanoporous gold. The lattice spacing of 0.29 and 0.32 nm in Figures 3c and 3d can be assigned to (130) and (021) plane of α-MoO_3 (JCPDS 05-0508, space group: Pbnm, a_0 = 3.962 Å, b_0 = 13.85 Å, and c_0 = 3.697 Å). Thus, both lattice fringe and EDX of TEM studies confirmed that MoO_3 nanoparticles were formed on the surface of np-Au ligaments after thermal treatment at 200°C in air.

10

The crystal structure of nanoporous gold catalyst (pure np-Au) was characterized with XRD technique. As shown in Figure 4a, five peaks centered at 38.3, 44.5, 64.6, 77.7, and 82° were assigned to (111), (200), (220), (311), and (222) plane of cubic phase gold metal (JCPDS 04-0784, space group: Fm-3m, $a_0 = b_0 = c_0 = 4.0786$ Å), respectively. After the integration of MoO_3 nanoparticles to the pores, the crystal structures of MoO_3@np-Au catalysts remained unchanged. For example, the crystal structures of MoO_3@np-Au catalysts with doping of 1.0wt% (Figure 4b) and 2.0wt% Mo (Figure S3) were nearly identical to that of pure nanoporous gold catalyst (Figure 4a) although MoO_3 nanoparticles were clearly observed by HRTEM (Figure 3); no diffraction peak of MoO_3 was observed in Figure 4a and Figure S3. The lack of diffraction peak in XRD of MoO_3 in the MoO_3@np-Au is due to the low loading of molybdenum. The molybdenum oxide modified nanoporous catalyst was further characterized by Raman spectroscopy. As shown in Figure S4, the peak at 990 cm^{-1} could be assigned to terminal Mo=O bond of MoO_3 nanoparticles.[48]

3.2 Selective oxidation of cyclohexene

The above prepared pure np-Au and MoO_3@np-Au were used for selective oxidation of cyclohexene in liquid phase under solvent free condition. Pure oxygen was used as the sole oxidant and tert-butyl hydroperoxide was used as the initiator. As shown in Figure 5 and entry 1 of Table 2, around 40% of cyclohexene was oxidized on the pure nanoporous gold catalyst at 90°C after reaction of 4 h. The high conversion results from the mechanism of radical chain reaction of oxidation of cyclohexene on pure np-Au as proposed in literature.[31,49]. The major product formed through the catalysis on pure nanoporous

gold was cyclohexenyl hydroperoxide; the selectivity for the desired cyclohexene oxide was only 7%. The catalytic performance on np-Au is consistent with literature results on cyclohexene oxidation over Au nanoparticles supported on SiO_2 under solvent-free condition by using molecular oxygen as oxidant.[31,35]

Compared to pure np-Au, the conversion of cyclohexene on 1wt%MoO$_3$@np-Au was dropped to around 4.4%, and the selectivity of cyclohexene oxide was significantly increased from 7% to about 61% (Figure 5 and Entry 2 in Table 2). Industrial transformation of cyclohexane is in fact processed at a low conversion in order to avoid formation of excessive undesired byproducts.[50,51] Thus, the conversion of cyclohexene of 4.4% is feasible for industrial production. In the blank experiment without using any catalyst, the major product formed was cyclohexenyl hydroperoxide. By comparing the blank experiment with pure nanoporous gold and MoO$_3$@np-Au catalysts (entry 11 vs entry 1 vs entry 2), it can be found that the selectivity of reaction products varied significantly at similar conversion of 3.2-4.4%. For blank experiment, no cyclohexene oxide was formed at conversion of 3.2%. With using pure nanoporous gold catalyst (np-Au-200°C-air), the selectivity of cyclohexene oxide was increased to 5.7%. By modification nanoporous gold with molybdenum oxide (1.0wt%MoO$_3$@np-Au-200°C-air), the selectivity of cyclohexene oxide was largely increased to 61.2%, which clearly demonstrate the importance of Mo and Au in shifting the products selectivity of cyclohexene oxidation. With further increase of the molybdenum loading to 2wt% (2.0wt%MoO$_3$@np-Au), the conversion of cyclohexene can increase to 11.1%, while the selectivity for production of cyclohexene oxide still maintained at about 58.6% (entry 3 of Table 2 and Figure 5). Compared to the high conversion of cyclohexene on pure np-Au, MoO$_3$@np-Au exhibit a low conversion of cyclohexene but much higher selectivity for production of cyclohexene oxide under the

exact same catalytic condition (reaction temperature, molecular oxygen, and solvent free). This distinct difference in catalytic performances between pure np-Au and Mo@np-Au suggests that MoO$_3$@np-Au catalyzes the selective oxidation of cyclohexene via a pathway different from the radical reaction route proposed for pure nanoporous gold catalyst in literature.[31,49] Hot filtration has been established as a standard method to test catalyst leaching.[52,53] In present work, the cyclohexene reaction was carried out in pressurized reactor, and it is difficult to apply the hot filtration method for the evaluation. Thus the molybdenum loading was examined before and after reaction to verify possible leaching of molybdenum oxide during reaction. As shown in Figure S4, the molybdenum content was similar before and after cyclohexene oxidation, which suggests that there is no or no significant leaching of molybdenum oxide during the reaction. Furthermore, molybdenum oxide is known to have negligible solubility in nonpolar solvent.[54] As nonpolar cyclohexene was used as reactant and solvent in the reaction, it further suggests that leaching of molybdenum oxide into cyclohexene is unlikely in present work. Furthermore, the carbon balance for the reaction over nanoporous gold catalysts has been calculated and presented in Table S1. As can be seen, the total carbon numbers before and after reaction are similar for pure and molybdenum oxide modified nanoporous gold catalysts, which suggests the major products of this reaction are oxygenated cyclohexenes.

Homogeneous molybdenum-based molecular catalyst can oxidize cyclohexene to cyclohexene oxide when peroxide was used as oxidant;[55,56] in this homogeneous catalysis, the key step is the activation of molybdenum atoms of the molecular catalyst by peroxide to form molybdenum oxo-peroxo species which act as active catalytic site for selective epoxidation of cyclohexene.[55,56] Inspired by the proposed pathway of Mo-based molecular catalyst for selective epoxidation of cyclohexene,[55,56] We have proposed a

13

pathway to rationalize the selective oxidation of cyclohexene to cyclohexene oxide over MoO_3@np-Au catalysts. As shown in Figure 6, the initial molybdenum peroxo species (a4 in Figure 6) was formed on polymeric molybdenum oxide through the reaction of initiator tert-butyl hydroperoxide with surface polymeric molybdenum oxide (a1 in Figure 6). The formed molybdenum peroxo species act as active sites. The peroxide oxygen atoms (-O-O-) of the molybdenum peroxo species (b1) attacked the double bond of cyclohexene directly to produce cyclohexene oxide (b3), by which the molybdenum peroxo species was reduced to b3 in Figure 6. The reduced form (b3 or c1 in Figure 6) can be oxidized by the oxygen activated by Au at the Au-MoO_3 interface (c2), restoring the catalytic site (c4) for next cycle of epoxidation of cyclohexane. In this pathway, the formation of cyclohexene oxide occurs at the interface of Au and MoO_3. As shown in Figures 3c and 3d, TEM studies revealed that the surface of nanoporous gold was partially covered by molybdenum oxide nanoparticles. Au-MO_3 interface can be clearly identified in Figures 3c and 3d. The region consisting of both MoO_3 nanoparticles and Au can be identified readily.

The effect of catalytic temperature on the conversion and selectivity was investigated by varying the reaction temperature from 80 to 100°C (Figure 7 and Table 2). As expected more cyclohexene was oxidized with the increase of temperature. For instance, the conversion of cyclohexene was increased to 36% at 100°C. Unfortunately, the selectivity for production of cyclohexene oxide at 100°C dropped significantly to 12.9%. Meanwhile, the selectivity for production of cyclohexenyl hydroperoxide at 100°C increased to 30.5% (entry 8 of Table 2). It seems that cyclohexenyl hydroperoxide accumulated very fast at 100°C (entry 8 of Table 2), and the reaction pathway switched to a radical chain mechanism at this

14

relatively high temperature. Thus, 80-90ºC is the optimum temperature at this catalytic condition which offer catalytic selectivity for production of epoxide of 58.6%-73%.

The effect of thermal treatment temperature of MoO_3@mp-Au before catalysis on its catalytic performance was investigated on MoO_3@np-Au annealed at 200ºC in air and MoO_3@np-Au annealed at 300ºC in air. As shown in Figure 8 and entry 4 of Table 2, the conversion of cyclohexene on 10 mg of 1.0wt%MoO_3@np-Au (annealed at 300ºC in air) increased to 43.2% in contrast to the catalyst annealed at 200ºC in air. However, the selectivity of cyclohexene oxide decreased largely to 16.1% and the selectivity of cyclohexenyl hydroperoxide increased to 43.6%. The decrease and increase of selectivity for production of epoxide and cyclohexenyl hydroperoxide, respectively on 1.0wt%MoO_3@np-Au (annealed at 300ºC in air)   suggests that the reaction pathway on the catalyst calcined at 300ºC in air follows a radical chain mechanism similar to that of catalyst MoO_3 supported on silica (entry 10, table 2)[31,49] In fact, TEM studies of MoO_3@np-Au (annealed at 300ºC in air) showed that the surface of the ligaments of this catalyst was nearly fully covered with molybdenum oxide nanoparticles (Figure 9), which minimized the interfacial sites of Au and MoO_3 nanoparticles since most Au surface was covered with MoO_3 nanoparticles. These MoO_3 nanoparticles formed an ultrathin film of MoO_3. Thus, it is reasonable to suggest that the MoO_3@mp-Au (annealing at 300ºC in air) behaves like a MoO_3 catalyst. The distinct different catalytic performance between MoO_3@np-Au calcined at 200ºC and 300ºC suggested that the molybdenum oxide/gold interface is critical for activation of molecular oxygen (c2 in Figure 6), by which the oxygen can be activated to generate active oxo-peroxo species on MoO_3 surface for the formation of cyclohexene oxide (c4 in Figure 6).

The effect of pretreatment condition was further studied by reducing the air calcined and as-synthesized Mo/npAu catalysts in hydrogen. As shown in entry 2 and entry 5 of Table 2, the conversion of cyclohexene was 4.4 and 5.3% for the catalyst treated at 200ºC in air and hydrogen at 200ºC respectively. The selectivity of cyclohexene oxide and cyclohexenol was 63.0 and 30.5% for npAu-200ºC H_2, which was similar as that of npAu-200 ºC in air. It suggested that oxidation or reduction atmosphere at 200 ºC has negligible effect on the catalytic performance. It was due to that only decomposition of ammonium heptamolybdate occurred at 200ºC, and reduction of molybdenum happened at a higher temperature (i.e., 300 ºC). For the Mo/npAu-200ºC-air-300ºC H_2, the selectivity of cyclohexene oxide was further increased to 73.1%, while the conversion of cyclohexene was kept as 3.5% (entry 6 of Table 2). The increased selectivity was possibly due to better dispersion of molybdenum oxide on the nanoporous gold surface, with help to hydrogen treatment at 300 ºC.

X-ray photoelectron spectroscopy was used to examine the oxidation state of Mo and Au of MoO$_3$@np-Au and pure np-Au. For pure np-Au, one photoemission feature of Au $4f_{7/2}$ was observed at 83.9 eV, which is typical for gold at a metallic state (Figure 10a); the O 1s peak appeared at 532.6 and 534.8 eV was attributed to surface hydroxyl group and adsorbed water, respectively (Figure 10b).[57] There was no N 1s peak observed from the wide scan XPS spectrum (Figure S5), which suggests that most of the surfactant (e.g., polyvinylpyrrolidone) used for preparation of nanoporous gold has been removed through washing and calcination steps.[58] For 1.0wt%MoO$_3$@np-Au annealed at 200ºC in air, the nanoporous gold was also in metallic state as evidenced by the Au $4f_{7/2}$ peak at 84.0 eV (Figure 11a). The fitted Mo $3d_{5/2}$ peak was centered at 232.2 eV, which was attributed Mo^{6+}.[56] The O 1s photoemission feature was deconvoluted into three peaks at 530.4, 532.8, and 534.3 eV, which could be assigned to

oxygen atoms of molybdenum oxide (530.4 eV), surface hydroxyl group (532.8 eV), and surface adsorbed waters (534.3 eV) species, respectively.[54,57,59] Thus, XPS studies confirmed the metallic state of Au in surface region and the valence state (VI) of MoO_3 nanoparticles for MoO_3@np-Au. Furthermore, no N 1s peak was observed in the wide scan (Figure S6), suggesting that most of the molybdenum precursor (ammonium heptamolybdate) was decomposed during thermal treatment in air.

Structure of the spent 1.0wt%MoO_3@np-Au catalysts was characterized by STEM/EDX analysis. As shown in Figure 12, the porous structure of 1.0wt%MoO_3@np-Au almost preserved after cyclohexene oxidation. The diameters of gold ligaments were about 20 nm, which was similar to that of catalyst before catalysis. Furthermore, the STEM/EDX showed that MoO_3 nanoparticles remained nearly uniformly dispersed on the nanoporous gold surface.

4. Conclusions

In summary, bi-functional catalyst 1.0wt%MoO_3@np-Au consisting of pores of nanoporous gold catalysts and MoO_3 nanoparticles anchored on surface of pores, were successfully synthesized via a wet chemistry synthetic route. On pure nanoporous gold catalyst, cyclohexene was mainly oxidized to cyclohexenyl hydroperoxide, which functioned as radical chain propagator to produce other oxidized products (i.e., cyclohexene oxide, cyclohexenol, and cyclohexenone) via radial chain mechanism. The integration of MoO_3 nanoparticles onto Au ligaments of nanoporous gold significantly increased the selectivity for production of epoxide in cyclohexene oxidation reaction. Selectivity for production of cyclohexene oxide up to 73% was achieved over 1.0wt%MoO_3@np-Au catalyst. It is expected that the

high selectivity of production of cyclohexene oxide on MoO$_3$@np-Au results from the formation of active sites, molybdenum peroxo species, which oxidize cyclohexene to cyclohexene oxide. The molybdenum peroxo species can be regenerated by oxygen activated by Au atoms at the interface of Au and MoO$_3$ nanoparticles supported on the surface Au ligaments in np-Au.

Acknowledgement

Appendix A. Supplementary data

Supplementary data associated with this article can be found, in the online version, at http://dx.doi.org/

References

1. G. Ertl, H. Knözinger, F. Schuth, J. Weitkamp, Handbook of Heterogeneous Catalysis, 2nd ed.; Wiley-VCH, 2008.

2. N. Mizuno, K. Yamaguchi, K. Kamata, Coord. Chem. Rev. 249 (2005) 1944-1956.

3. J. R. Monnier, Appl. Catal. A 221 (2001) 73-91.

4. M. L. Kuznestsov, B. G. M. Rocha, A. J. L. Pombeiro, G. B. Shul'pin, ACS Catal. 5 (2015) 3823-3835.

5. V. Escande, E. Petit, L. Garoux, C. Boulanger, C. Grison, ACS Sustainable Chem. Eng. 3 (2015) 2704-2715.

6. S. Gupta, C. P. Vinod, D. Jagadeesan, RSC Adv. 5 (2015) 92371-92377.

7. M. Liu, X. Z. Wang, Y. Q. Chen, L. Y. Dai, RSC Adv. 5 (2015) 61481-61485.

8. G. Anilkumar, B. Bitterlich, F. G. Gelalcha, M. K. Tse, M. Beller, Chem. Commun. (2007) 289-291.

9. P. P. Pescarmona, J. V. Noyen, P. A. Jacobs, J. Catal. 251 (2007) 307-314.

10. S. Rahman, S. A. Farooqui, A. Rai, R. Kumar, C. Santra, V. C. Prabhakaran, G. R. Bhadu, D. Sen, S. Mazumder, S. Maity, A. K. Sinha, B. Chowdhury, RSC Adv. 5 (2015) 46850-46860.

11. J. W. Brown, Q. T. Nguyen, T. Otto, N. N. Jarenwattananon, S. Glöggler, L. S. Bouchard, Catal. Commun. 59 (2015) 50-54.

12. S. Sha, H. Yang, J. Li, C. F. Zhuang, S. Gao, S. X. Liu, Catal. Commun. 43 (2014) 146-150.

13. Z. F. Li, S. J. Wu, H. Ding, D. F. Zheng, J. Hu, X. Wang, Q. S. Huo, J. Q. Guan, Q. B. Kan, New J. Chem. 37 (2013) 1561-1568.

14. I. Y. Skobelev, A. B. Sorokin, K. A. Kovalenko, V. P. Fedin, O. A. Kholdeeva, J. Catal. 298 (2013) 61-69.

15. C. S. Alvarez, F. García, S. M. Humphrey, A. D. Hopkins, R. A. Kowenicki, M. McPartlin, R. A. Layfield, R. Raja, M. C. Rogers, A. D. Woods, D. S. Wright, Chem. Commun. (2005) 198-200.

16. M. A. Cinellu, G. Minghetti, F. Cocco, S. Stoccoro, A. Zucca, M. Manassero, Angew. Chem. Int. Ed. 44 (2005) 6892-6895.

17. R. J. Chimentão, I. Kirm, F. Medina, X. Rodríguez, Y. Cesteros, P. Salagre, J. E. Sueiras, Chem. Commun. (2004) 846-847

18. M. D. Hughes, Y.-J. Xu, P. Jenkins, P. McMorn, P. Landon, D. I. Enache, A. F. Carley, G. A. Attard, G. J. Hutchings, F. King, E. H. Stitt, P. Johnston, K. Griffin, C. J. Kiely, Nature 437 (2005) 1132-1135.

19. Y. Y. Fang, Y. Z. Chen, X. Z. Li, X. C. Zhou, J. Li, W. J. Tang, J. W. Huang, J. Jin, J. T. Ma, J. Mol. Catal. A 392 (2014) 16-21.

20. P. Bujak, P. Bartczak, J. Polanski, J. Catal. 295 (2012) 15-21.

21. L. Wang, H. Wang, P. Hapala, L. F. Zhu, L. M. Ren, X. J. Meng, J. P. Lewis, F.-S. Xiao, J. Catal. 281 (2011) 30-39.

22. Y. Yao, X. M. Zhang, J. Peng, Q. H. Yang, Chem. Commun. 51 (2015) 3750-3753.

23. H. Alshammari, P. J. Miedziak, T. E. Davies, D. J. Willock, D. W. Knight, G. J. Hutchings, Catal. Sci. Technol. 4 (2014) 908-911.

24. C. O. L. Crites, G. L. Hallet-Tapley, M. González-Béjar, J. C. Netto-Ferreira, J. C. Scaiano, Chem. Commun. 50 (2014) 2289-2291.

25.   E. Tebandeke, C. Coman, K. Guillois, G. Canning, E. Ataman, J. Knudsen, L. R. Wallenberg, H. Ssekaalo, J. Schnadt, O. F. Wendt, Green Chem. 16 (2014) 1586-1593.

26.   L. Hu, X. Q. Cao, J. H. Yang, M. Li, H. Y. Hong, Q. F. Xu, J. F. Ge, L. H. Wang, J. M. Lu, L. Chen, H. W. Gu, Chem. Commun. 47 (2011) 1303-1305.

27.   M. Boualleg, K. Guillois, B. Istria, L. Burel, L. Veyre, J.-M. Basset, C. Thieuleux, V. Caps, Chem. Commun. 46 (2010) 5361-5363.

28.   M. Turner, V. B. Golovko, O. P. H. Vaughan, P. Abdulkin, A. Berenguer-Murcia, M. S. Tikhov, B. F. G. Johnson, R. M. Lambert, Nature 454 (2008) 981-984.

29.   X. Y. Deng, C. M. Friend, J. Am. Chem. Soc. 127 (2005) 17178-17179.

30.   J. Fang, B. Zhang, Q. Yao, Y. Yang, J. Xie, N. Yan, Coord. Chem. Rev. 322 (2016) 1-29.

31.   B. G. Donoeva, D. S. Ovoshchnikov, V. B. Golovko, ACS Catal. 3 (2013) 2986-2991.

32.   Z.-Y. Cai, M.-Q. Zhu, J. Chen, Y.-Y. Shen, J. Zhao, Y. Tang, X.-Z. Chen, Catal. Commun. 12 (2010) 197-201.

33.   M. S. Nejad, G. Ghasemi, M. V. Martínez-Huerta, M. Ghiaci, J. Mol. Catal. A 406 (2015) 118-126.

34.   Y. X. Zhang, X. Han, R. H. Liu, Y. Liu, H. Huang, J. M. Zhang, H. Yu, Z. H. Kang, J. Phys. Chem. C 116 (2012) 20363-20367.

35.   D. S. Ovoshchnikov, B. G. Donoeva, B. E. Williamson, V. B. Golovko, Catal. Sci. Technol. 4 (2014) 752-757.

36.   B. Zhang, H. Asakura, J. Zhang, J. Zhang, S. De, N. Yan, Angew. Chem. Int. Ed. 55 (2016) 8319-8323.

37.   A. S. Touchy, S. M. A. H. Siddiki, W. Onodera, K. Kon, K. Shimizu, 18 (2016) 2554-2560.

38. C. Sener, T. S. Wesley, A. C. Alba-Rubio, M. D. Kumbhalkar, S. H. Hakim, F. H. Ribeiro, J. T. Miller, J. A. Dumesic, ACS Catal. 6 (2016) 1334-1344.

39. R. Carrasquillo-Flores, I. Ro, M. D. Kumbhalkar, S. Burt, C. A. Carrero, A. C. Alba-Rubio, J. T. Miller, I. Hermans, G. W. Huber, J. A. Dumesic, J. Am. Chem. Soc. 137 (2015) 10317-10325.

40. Z. Liu, J. E. Hu, Q. Wang, K. Gaskell, A. I. Frenkel, G. S. Jackson, B. Eichhorn, J. Am. Chem. Soc. 131 (2009) 6924-6925.

41. A. Wittstock, M. Bäumer, Acc. Chem. Res. 47 (2014) 731-739.

42. X. M. Zhang, Y. Ding, Catal. Sci. Technol. 3 (2013) 2862-2868.

43. Y. X. Zhang, H. C. Zeng, Int. J. Nanotechnol. 8 (2011) 816-824.

44. R. D. Mair, A. J. Graupner, Anal. Chem. 36 (1964) 194-204.

45. J. L. Wang, R. Xia, J. J. Zhu, Y. Ding, X. Zhang, Y. F. Chen, J. Mater. Sci. 47 (2012) 5013-5018.

46. Y. H. Tan, J. A. Davis, K. Fujikawa, N. V. Ganesh, A. V. Demchenko, K. J. Stine, J. Mater. Chem. 22 (2012) 6733-6745.

47. R. Li, K. Sieradzki, Phys. Rev. Lett. 68 (1992) 1168-1171

48. J. Dou, H. C. Zeng, J. Am. Chem. Soc. 134 (2012) 16235-16246.

49. M. Conte, X. Liu, D. M. Murphy, K. Whiston, G. J. Hutchings, Phys. Chem. Chem. Phys. 14 (2012) 16279-16285.

50. B. P. C. Hereijgers, R. F. Parton, B. M. Weckhuysen, ACS Catal. 1 (2011) 1183-1192.

51. I. Hermans, P. Jacobs, J. Peeters, Chem. Eur. J. 13 (2007) 754-761.

52. R. A. Sheldon, M. Wallau, I. W. C. E. Arends, U. Schuchardt, Acc. Chem. Res. 31 (1998) 485-493.

53. I. W. C. E. Arends, R. A. Sheldon, Appl. Catal. A 212 (2001) 175-187.

54.   J. Dou, H. C. Zeng, ACS Catal. 4 (2014) 566-576.

55.   P. Chandra, S. L. Pandhare, S. B. Umbarkar, M. K. Dongare, K. Vanka, Chem. Eur. J. 19 (2013) 2030-2040.

56.   D. V. Deubel, G. Frenking, P. Gisdakis, W. A. Herrmann, N. Rösch, J. Sundermeyer, Acc. Chem. Res. 37 (2004) 645-652.

57.   D. E. King, J. Vac. Sci. Technol. A 13 (1995) 1247-1253.

58.   B. Zhang, J. Fang, J. Li, J. J. Lau, D. Mattia, Z. Zhong, J. Xie, N. Yan, Chem. Asian J. 11 (2016) 532-539.

59.   Z. Song, J. Hrbek, R. Osgood, Nano Lett. 5 (2005) 1327-1332.
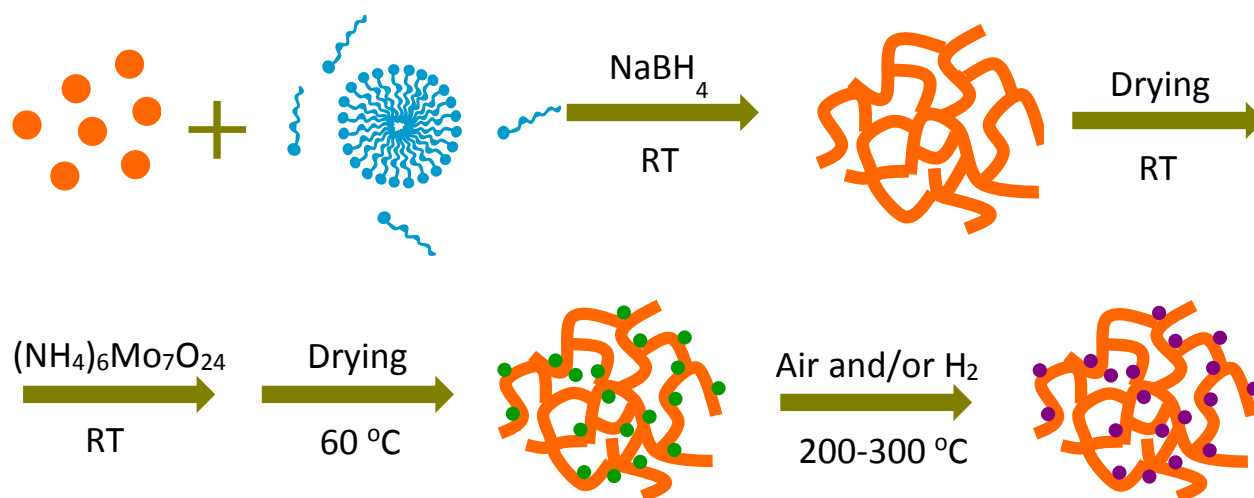
Figure 1. Scheme of synthesis of catalyst integrating nanoporous Au with MoO$_3$ nanoparticles.
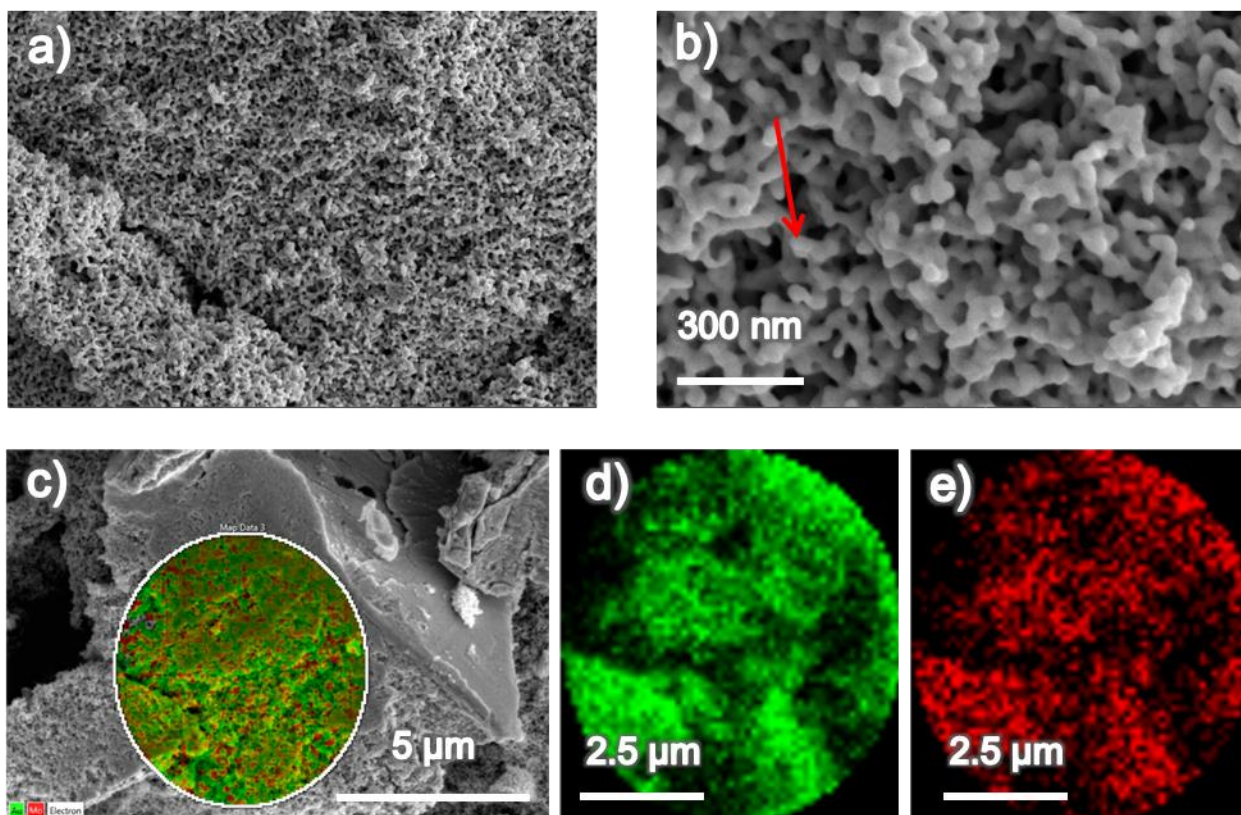
Figure 2. (a, b) SEM images and (c-e) EDX mapping of 1.0wt%MoO$_3$@np-Au (annealed at 200°C in air). The red arrow in (b) marks one ligament in a pore of 1.0wt%MoO$_3$@np-Au

.
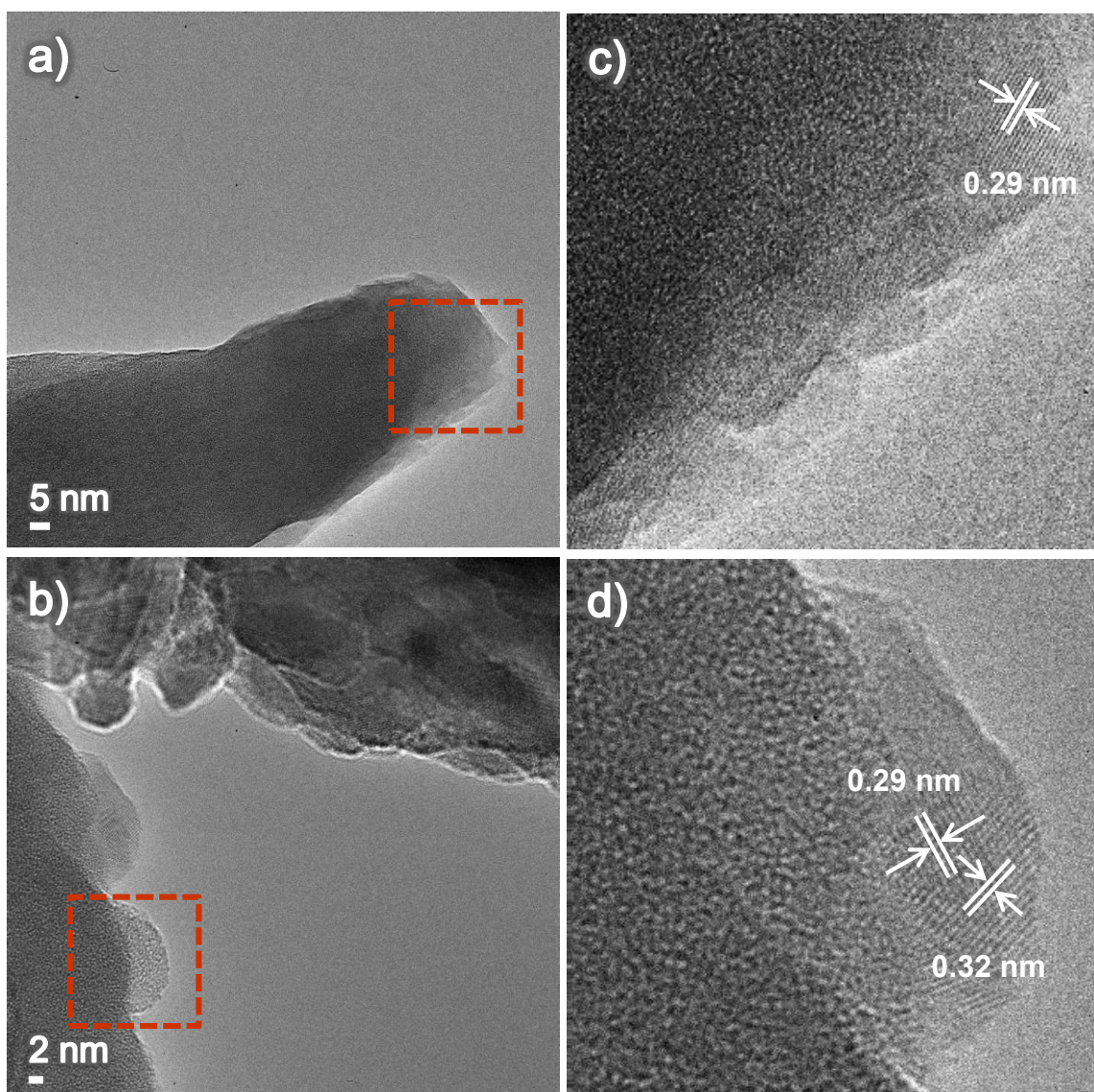
Figure 3. (a, b) HRTEM images of 1.0wt%MoO$_3$@np-Au (annealed at 200°C in air) and (c, d) visual enlargement of the selected sections in (a) and (b).
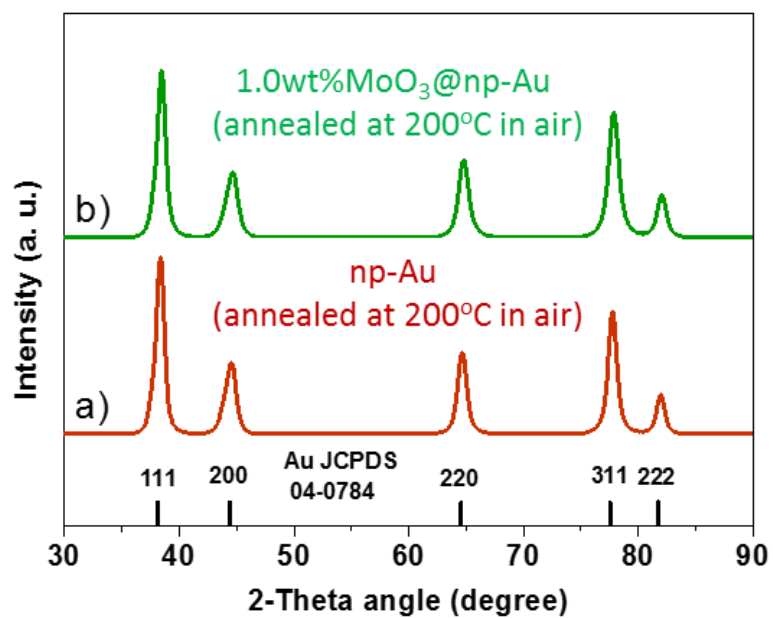
Figure 4. XRD patterns of (a) pure nanoporous gold (np-Au) and (b) 1.0wt%MoO3@np-Au (annealed at 200ºC in air).

27
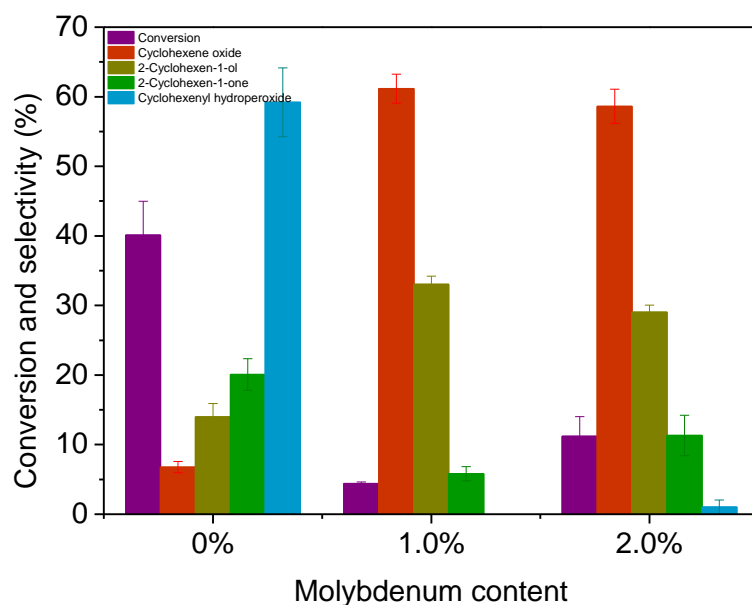
Figure 5. Selective oxidation of cyclohexene over catalysts of MoO$_3$@np-Au annealed at 200ºC in air The X-axis is the concentrations of three catalysts including pure np-Au, 1.0wt%MoO$_3$@np-Au (annealed at 200ºC in air), 2.0wt%MoO$_3$@np-Au (annealed at 200ºC in air). Reaction condition: 15 ml cyclohexene, 0.5 ml undecane (internal standard), 0.27 ml tert-butyl hydroperoxide, 10mg catalyst, 4 bar O$_2$, catalysis temperature: 90ºC, catalysis time: 4 h.
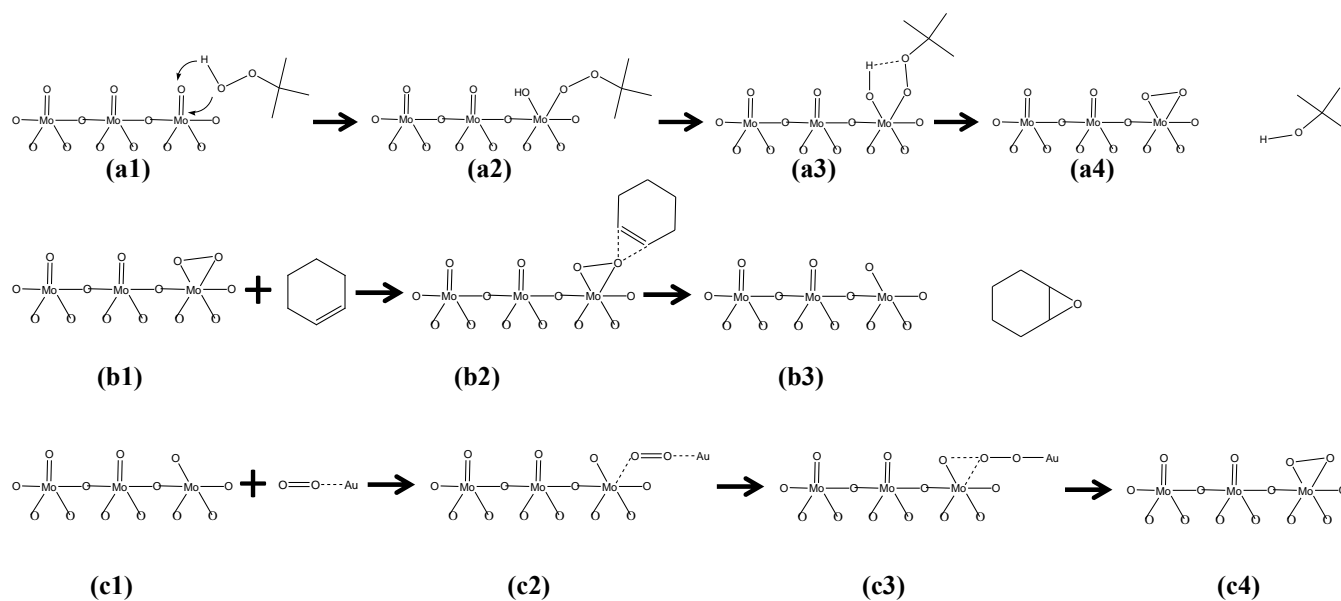
**Figure 6.** Suggested pathway for epoxidation of cyclohexene over MoO$_3$@np-Au catalyst.
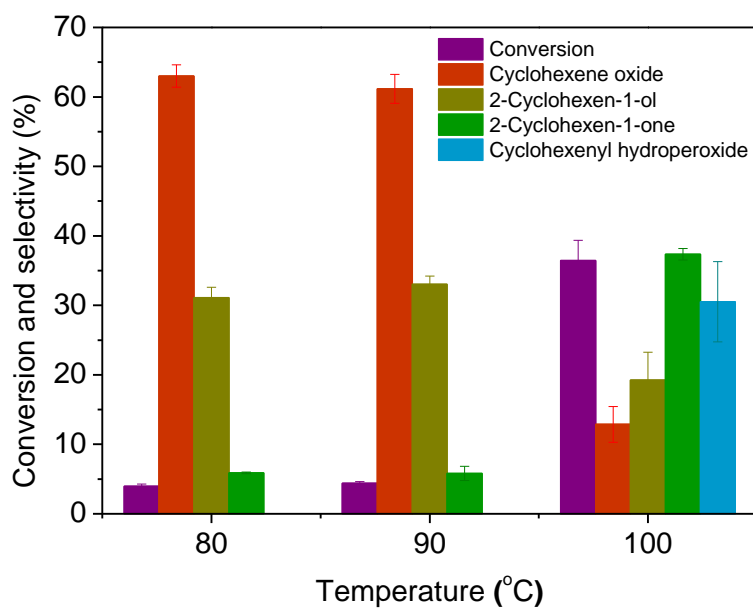
Figure 7. Selective oxidation of cyclohexene at different temperatures over 1.0wt%MoO$_3$@np-Au (annealed at 200°C in air). X-axis is the catalytic temperatures of selective oxidation of cyclohexene. Reaction condition: 15 ml cyclohexene, 0.5 ml undecane (internal standard), 0.27 ml tert-butyl hydroperoxide, 10 mg catalyst, 4 bar O$_2$, catalysis temperature: 80-100°C, catalysis time: 4 h.
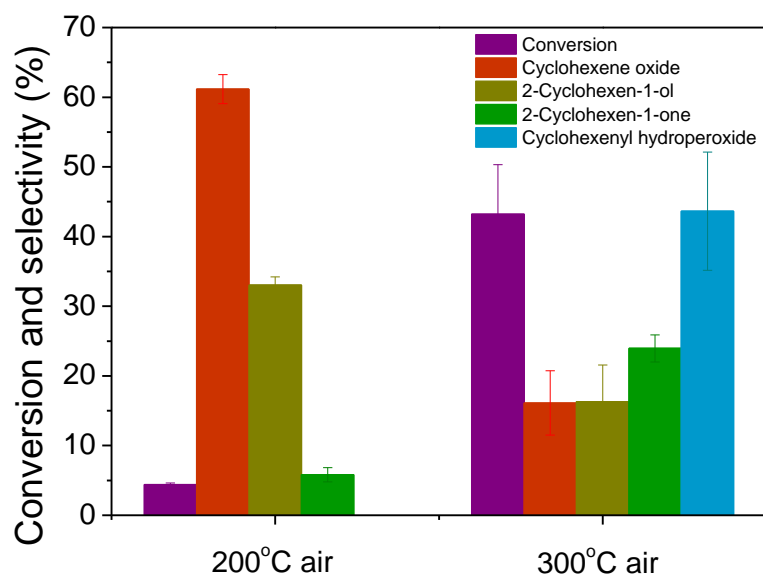
Figure 8. Selective oxidation of cyclohexene over 1.0wt%MoO$_3$@np-Au catalysts (annealed at 200°C or 300°C in air). The X-axis is the annealing temperature of catalysts in air before catalysis. Reaction condition: 15 ml cyclohexene, 0.5 ml undecane (internal standard), 0.27 ml tert-butyl hydroperoxide, 10 mg catalyst, 4 bar O$_2$, catalysis temperature: 90°C, catalysis time: 4 h.

Figure 9. TEM image of 1.0wt%MoO_3@np-Au (annealed at 300°C in air). Basically, most surface of the Au ligaments in np-Au was covered with MoO_3 nanoparticles.
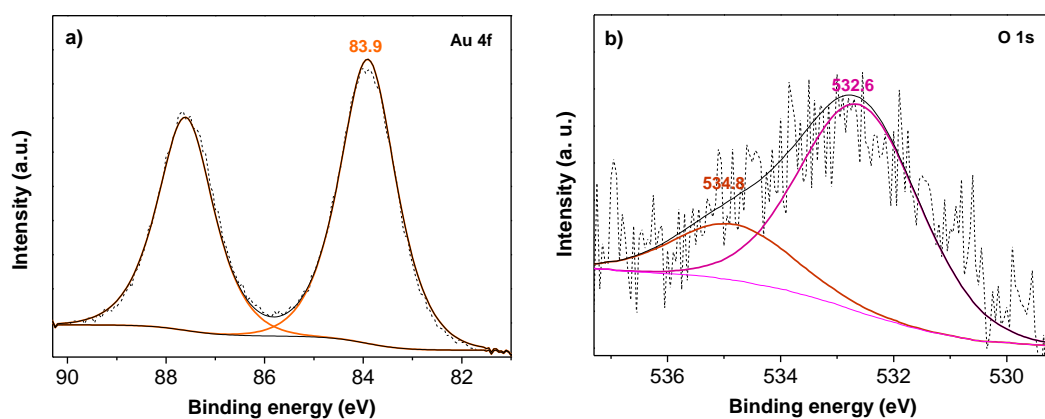
Figure 10. XPS spectra of (a) Au 4f and (b) O 1s of np-Au (annealed at 200ºC in air).
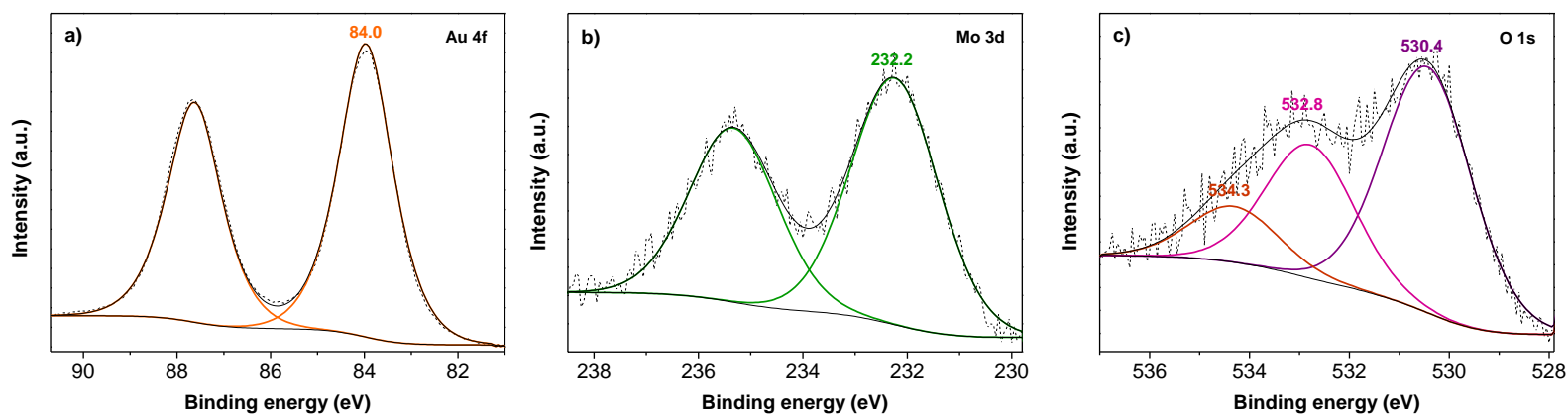
Figure 11. XPS spectra of (a) Au 4f, (b) Mo 3d and (c) O 1s of 1.0wt%MoO$_3$@np-Au (annealed at 200°C in air).
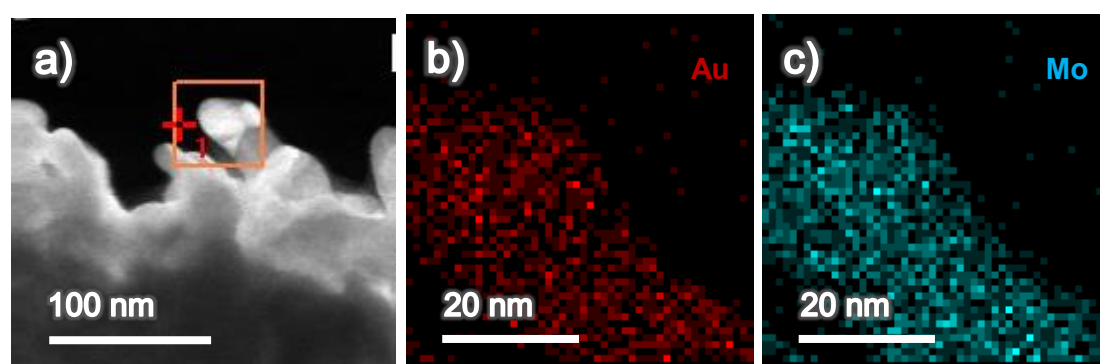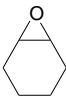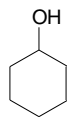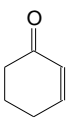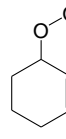
Figure 12. (a) STEM image and (b, c) EDX mapping of 1.0wt%MoO$_3$@np-Au (annealed at 200ºC in air) after catalysis of cyclohexene oxidation.

Table 1. Physical properties of MoO_3@np-Au catalysts

Catalyst	Mo loading (wt%)	BET surface area (m^2/g)	Pore volume (mL/g)
np-Au	0	2.9	0.078
1.0wt%MoO₃@np-Au	0.98	2.8	0.047
2.0wt%MoO₃@np-Au	2.05	2.3	0.023

Table 2. Selective oxidation of cyclohexene over Mo@np-Au nanoporous catalysts[a]

Entry	Catalyst	Temperature (°C)	Conversion [b] (%)	Selectivity (%) [c]			
				(epoxide)	(OH)	(=O)	(O-OH)
1	pure np-Au-200°C-air	90	4.7 [d]	5.7	8.9	7.2	78.1
			40.1	6.8	14.0	20.1	59.2
2	1.0wt%MoO$_3$@np-Au-200°C-air	90	4.4	61.2	33.0	5.8	0
3	2.0wt%MoO$_3$@np-Au-200°C-air	90	11.1	58.6	29.0	11.3	1.0
4	1.0wt%MoO$_3$@np-Au-300°C-air	90	43.2	16.1	16.3	24.0	43.6
5	1.0wt%MoO$_3$@np-Au-200°C H$_2$	90	5.5	63.0	30.5	6.5	0
6	1.0wt%MoO$_3$@np-Au-200°C-air-300°C H$_2$	90	3.5	73.1	25.8	1.1	0
7	1.0wt%MoO$_3$@np-Au-200°C-air	80	3.9	63.0	31.1	5.9	0
8	1.0wt%MoO$_3$@np-Au-200°C-air	100	36.4	12.9	19.2	37.4	30.5
9	1.0wt%MoO$_3$@np-Au-200°C-air [e]	100	2.5	46.5	41.0	12.5	0
10	1.0wt%MoO$_3$/Al$_2$O$_3$-200°C-air	90	29.0	22.6	20.2	27.5	29.7
11	Blank [f]	90	1.1 [g]	0.0	0.0	12.9	87.1
12	Blank	90	3.2 [h]	0.0	5.7	11.4	82.8

Notes: [a] Reaction condition: 15 ml cyclohexene, 0.5 ml undecane (internal standard), 0.27 ml tert-butyl hydroperoxide, 10mg catalyst, 4 bar O$_2$, catalysis temperature: 90°C, catalysis time: 4 h. [b] Conversion was calculated using total oxidation products produced divided by initial amount of cyclohexene. [c] Selectivity was calculated as individual product divided by total products formed. [d] Conversion at 0.5 h. [e] Without *tert*-butyl hydroperoxide. [f] Without using catalyst. [g] Conversion at 0.5 h. [h] Conversion at 1 h.